Sensors & Actuators: A. Physical 347 (2022) 113946

Contents lists available at ScienceDirect

Sensors and Actuators: A. Physical

journal homepage: www.journals.elsevier.com/sensors-and-actuators-a-physical

Magnetic binary encoding system based on 3D printing and GMI detection prototype

J.J. Beato-López [a,b,*], J.M. Algueta-Miguel [c,d], I. Galarreta-Rodriguez [a,b], A. López-Ortega [a,b], E. Garaio [a,b], C. Gómez-Polo [a,b], M. Aresti [e], E. Soria-Picón [e], J.I. Pérez-Landazábal [a,b]

[a] Dpto. de Ciencias, Universidad Pública de Navarra, 31006 Pamplona, Spain
[b] Institute for Advanced Materials and Mathematics INAMAT^2, Universidad Pública de Navarra, 31006 Pamplona, Spain
[c] Dpto.de Ingeniería Eléctrica, Electrónica y Comunicación, Universidad Pública de Navarra, 31006 Pamplona, Spain
[d] Institute of Smart Cities, Universidad Pública de Navarra, 31006 Pamplona, Spain
[e] NAITEC-Technological Center of Automotive and Mechatronics, C/Tajonar 20, 31006 Pamplona, Spain

ARTICLE INFO

Keywords:
3D printing
Polymer-matrix composites
Binary encoding information
GMI effect
Magnetic sensor
Electronic sensor interface

ABSTRACT

In this work, the feasibility of a magnetic binary encoding system using 3D printing technology is analyzed. The study has a double interest, that is, the possibility of printing a 3D piece that contains the codified information and the development of a system for its decoding. For this purpose, magnetic nanoparticles (magnetite Fe_3O_4) were embedded in a polymeric matrix of Polylactic Acid (PLA) and Poly-ε-caprolactone (PCL). Similar to a conventional barcode, a rectangular piece with an alternating pattern of strips with absence (only polymer) and a 5 wt% of embedded magnetic nanoparticles was 3D printed employing the Fused Deposition Modelling technique (FDM). The information was decoded by means of a Giant Magnetoimpedance (GMI) sensor-based prototype, by scanning the surface of the piece and measuring the changes in the magnetic field. As sensor nucleus, an amorphous soft magnetic wire of nominal composition $(Co_{0.94}\ Fe_{0.06})_{72.5}\ Si_{12.5}\ B_{15}$ was employed. The decoding prototype incorporates a homemade electronic sensor interface that permits, at the time, the GMI sensor excitation and the subsequent signal conditioning to optimize its response. The output signal enables the detection of the magnetite nanoparticles and the magnetic decoding of the encoded information ("1" and "0", presence or absence of the magnetic nanoparticles, respectively).

1. Introduction

The research of novel and functional magnetic materials has recently become a relevant research topic [1]. As a result of their relevant features related to their, generally speaking, fast, long-range and precise response in different environments [2], these materials have been implemented in new devices and applied in emerging technologies such as controlled motion [3], [4], mechanical reinforcement [5], [6], strain sensors [7], [8], and biomedical applications [9], [10] among others. In this sense, different magnetic devices have been developed based on the combination of distinct materials and the use of sophisticated structural geometries, showing an optimal performance under different conditions at various applications [2]. Some examples of this kind of devices can be found in the bibliography, for example, transformers [11], microfluidic platforms [12] and magnetic actuators [8], [13], etc. Anyway, the development of new structures requires novel manufacturing procedures that allow overcoming the constraints that exhibit the traditional fabrication strategies, mainly based on the predominant subtractive manufacturing processes. Under these principles, 3D printing represents a promising technique for a rapid and self-customized manufacturing of these complex magnetic (and non-magnetic) structures or geometries [2], [14]. This interdisciplinary technology consists of a two-step process. Initially, a computer-assisted 3D model is developed. Then the final printing process is carried out leading to a final 3D object. This stage consists of the successive deposition of thin layers of materials upon each other [15], [16]. Different materials are used in 3D printing, namely plastic, resins, rubbers, biomaterials, ceramics, glass, metals, etc [17]. So, among others, the advantages of this technique include the development of devices with complex internal structures (hollow and filled parts), the use of a wide variety of materials (single or composite), rapid and low-cost prototyping and a high level of personalization, allowing a fast adaptation to the requirements of the desired

* Corresponding author at: Dpto. de Ciencias, Universidad Pública de Navarra, 31006 Pamplona, Spain.
E-mail address: juanjesus.beato@unavarra.es (J.J. Beato-López).

https://doi.org/10.1016/j.sna.2022.113946
Received 19 July 2022; Received in revised form 27 September 2022; Accepted 14 October 2022
Available online 17 October 2022

application in almost any environment and available also for general public [1,17].

In this work, the feasibility of 3D printed magnetic composites (Fused Deposition Modelling, FDM) for binary encoding has been analyzed. To this end, magnetic composites that consist of nanometric commercial Fe_3O_4 particles (MNPs), i.e., 50–100 nm, were embedded in a semi-crystalline, biocompatible and biodegradable polymeric blend made of a Polylactic Acid (PLA) and Poly-ε-caprolactone (PCL). A rectangular-shaped piece was printed (similar to a visual conventional barcode), being formed by 4 strips with the same dimensions. An alternating pattern was chosen, where a polymeric strip (no MNPs) was followed by another with embedded MNPs and so on. Consequently, the encoding principle is derived from the capacity of detecting the MNPs presence, "1", or their absence, "0" when a magnetic sensor scans over the printed piece surface.

Derived from the low MNPs concentrations involved, a detection system based on the Giant Magnetoimpedance effect (GMI) was proposed. This effect consists of the huge changes in the high-frequency electrical impedance, Z, experienced by a soft magnetic conductor under an external magnetic field [18], such as the one generated by the MNPs. Its employment is justified by the larger sensitivity exhibited when compared to other magnetic detecting principles [19]. In those terms, previous GMI-based sensors for MNPs detection have been successfully developed [20], [21], [22]. More concretely, we have previously analyzed this topic using different geometries as ribbons [23], [24] and wires for the contactless and reusable detection [25] of the magnetic particles. In this work, a detection system is analyzed based on the voltage (amplitude), V, variations ($V \propto Z$) underwent by an amorphous wire of nominal composition $(Co_{0.94}Fe_{0.06})_{72.5}Si_{12.5}B_{15}$, while scanning over the 3D barcoded piece. The final prototype is completed by the addition of a homemade electronic sensor interface that permits, simultaneously, the sensor excitation and the signal conditioning to optimize its response.

2. Materials and methods

2.1. Preparation of magnetic composites

The fabrication of 3D printable filaments was initially addressed. Thus, a concentration of 5 wt% of iron oxide magnetic nanoparticles (Fe_3O_4) were embedded in a polymeric matrix with 90% PCL and 10% PLA. Commercial Fe_3O_4 MNPs (Sigma Aldrich, 637106), i.e., 50–100 nm were used for the composite fabrication. Fig. 1 shows the hysteresis loop measured with a homemade Vibrating-sample magnetometer (VSM) under a maximum applied field of 1.2 MA/m. As can be observed in the inset of Fig. 1, a non-zero value of the remanent magnetization (∼ 5.5 emu/g) was found for this situation. Although the MNPs are within the limit of superparamagnetic behavior [26], the occurrence of particle size dispersion caused that some nanoparticles could display a certain magnetization even at zero applied external magnetic field.

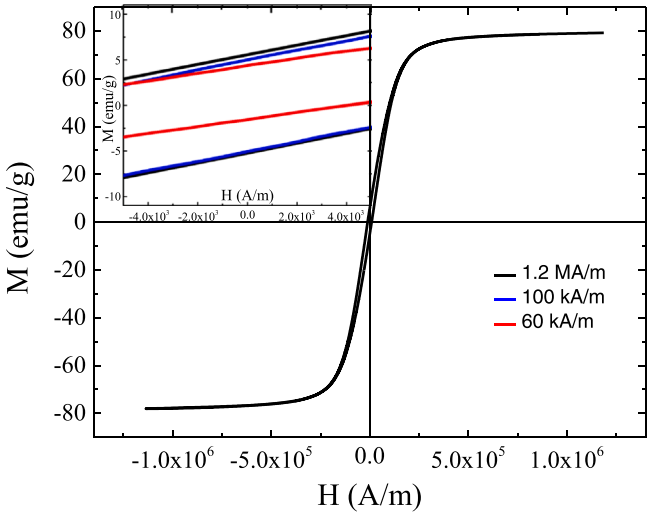

Fig. 1. Hysteresis loop at room temperature of commercial magnetite MNPs. Inset. Enlargement of the low magnetic field region for the different hysteresis loops measured at different maximum applied fields: 1.2 MA/m, 100 kA/m and 60 kA/m.

The solution casting method was used for the synthesis of homogeneous magnetic composites [27]. The following reagents were used: Polylactic acid (PLA, average molecular weight [Mw]≈ 144.000, Natureworks, USA), Polycaprolactone (PCL, average molecular weight [Mw]≈ 50.000, Polymorph, UK), magnetic iron oxide nanoparticles and dichloromethane (DCM) solvent both purchased from Sigma Aldrich. Briefly, PLA was dissolved in 300 mL of DCM with mechanical stirring at 30 ºC. As the PLA was dissolved, PCL was added. To promote a homogeneous mixture between both polymers, the solution was stirred vigorously for 2 h. Then magnetite nanoparticles were added. Stirring was kept for one more hour. Finally, the temperature was increased to 45 °C to facilitate the evaporation of DCM solvent, obtaining a composite precursor with a foam texture (see Fig. 2a). The final step was the PLA/PCL/MNPs filament extrusion. The fabrication of magnetic filaments was carried out using an extruder (FelFil Evo) with a 1.75 mm circular cross-section nozzle. The extrusion temperature was 80 ºC. An example of the printable 3D filament is shown in Fig. 2b.

2.2. Printing of 3D piece

With the developed printable filament, a magnetic barcode piece was 3D printed by FDM technique. The piece was fabricated by NAITEC, Technological Centre of Mobility and Mechatronics of Navarre, using a Raise 3D E2 printer with two print heads (dual extruders), one for the magnetic filament and the other for the pure polymeric matrix. As shown (see Fig. 3), the rectangular-shaped piece was comprised of 4 strips with an alternating pattern of absence and presence of MNPs. All strips exhibited the same dimensions, namely, 10 mm of length (x-direction), 4 mm of width (y-direction) and 2 mm of thickness (z-direction).

2.3. GMI Sensor treatment

The GMI sensing element is based on a soft magnetic amorphous wire $(Co_{0.94}\ Fe_{0.06})_{72.5}Si_{12.5}B_{15}$ obtained by "in-rotating-water-quenching" [28]. Initially, a 5 cm in length and 140 μm of diameter wire was sequentially current annealed ($t = 5$ min, $j = 19.5$ A/mm^2) and submitted to torsional strain, ranging from $\xi = 0$ to 10π rad/m, to induce a helical anisotropy on the sample [29]. Under a voltage divider configuration, the evolution of the sensor voltage, V, was characterized as a function of the external DC magnetic field, H, after each thermal-torsional treatment. The magnetic field was applied along the wire axis and generated by a pair of Helmholtz coils ($H = (583\frac{Am^{-1}}{A} \bullet I(A); I$ electrical current coil of radius $R = 4.5$ cm). The sensor was excited under conditions that optimized the GMI effect, namely, under a frequency of f= 100 kHz and peak-to-peak current intensity, I_{pp}= 20 mA. To this end, a standard signal generator (Standford Research Systems DS 345) was employed, being the sinusoidal AC signal amplitude measured with an AC current probe (Tektronix P6021). Voltage variations, V, were registered with a commercial lock-in amplifier (Standford Research Systems SR 844) as a function of H. It must be pointed out that the treatment of the wire was performed to enhance its GMI sensitivity in the low magnetic field region. As Fig. 4 demonstrates, due to the reinforcement of the helical anisotropy with the torsion angle during the current annealing, the position (applied H field) of the maximum of the GMI voltage shifts towards higher magnetic field values, ± 90 A/m. Moreover, a progressive enhancement of the

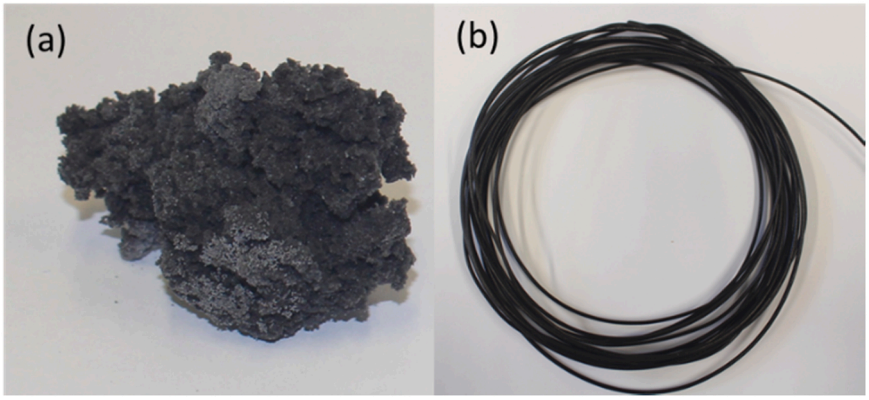

Fig. 2. a) Foam 3D filament precursor after chemical synthesis and b) 3D printable filament with MNPs embedded (5% wt).

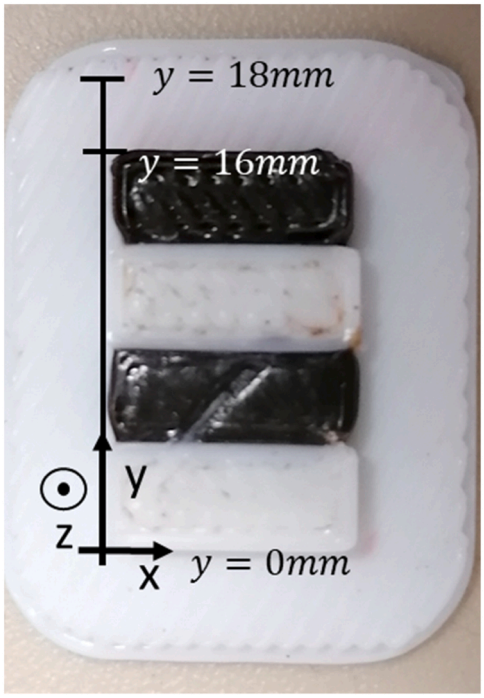

Fig. 3. Barcode patterned 3D printed piece.

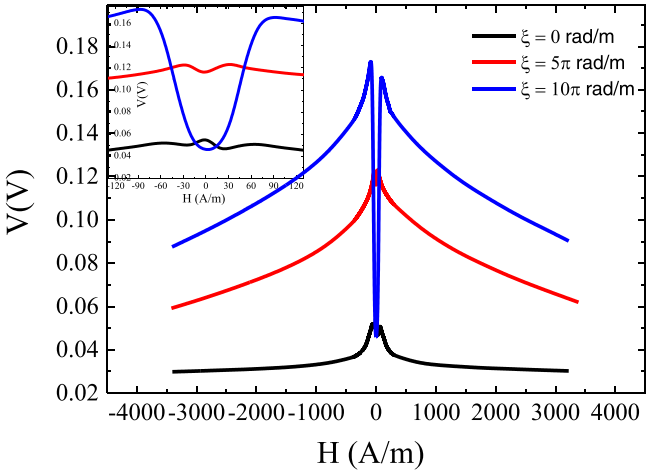

Fig. 4. Evolution of the 5 cm wire voltage, V, with external magnetic field, H in the initial as-quenched state and after successive current annealing treatment under different torsional strain, ξ.

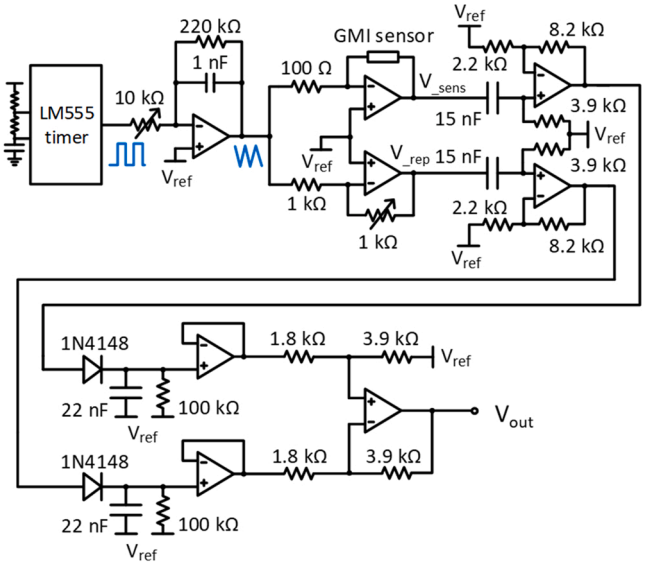

Fig. 5. Complete electronic sensor interface, including excitation signal generation and envelope detection circuit to obtain the output DC voltage.

sensitivity (higher slope) and an enlargement of the H range with linear sensor response, resulted in increasing applied torsional strains (see inset of Fig. 4) leading to a final mean sensitivity of 2×10^{-3} V/Am^{-1} (or 0.16 V/Oe). For sensing purposes, a piece of 10 mm twisted $\xi = 10\pi$ rad/m of the annealed wire was cut to perform the MNPs detection stage through the 3D piece surface scan.

2.4. Electronic sensor interface

The detection system consisted of an analog interface for both the excitation of the sensor and the signal conditioning of the GMI voltage. The complete scheme is shown in Fig. 5. The homemade designed electronic system was implemented in a breadboard using a single supply voltage of 5 V and a virtual ground *Vref* at 2.5 V. Operational amplifiers AD823 of Analog Devices were employed. The system consisted of three different blocks: the excitation signal generation, the sensing stage and an envelope detector that provided the final output *DC* voltage, V_{out}. A LM555 timer was used for generating a 100 kHz square signal, which was subsequently integrated to obtain a triangular waveform. This triangular signal is converted to current ($f = 100$ kHz and I_{pp}

= 20 mA) and applied to the sensor by using a transimpedance amplifier configuration. The excitation current was set by a variable resistor that controls the voltage gain of the opamp-based integrator.

The sensor output voltage, $V_{\_}$, ($V_{\_} \propto (I_{pp} \bullet Z)$) was amplified utilizing an *AC*-coupled non-inverter amplifier and the amplitude of the resulting voltage is measured employing a simple envelope detector, using 1N4148 diodes. The non-inverting amplifier has a double function: on the one hand, removing the possible *DC* offsets previously introduced by the setup, and on the other hand, ensuring an output signal amplitude large enough for dealing with the dropout voltage of the passive diodes.

Note that a replica of the main branch was added in parallel to the sensing circuit. This extra circuitry aimed to obtain a reference voltage, $V_{\_}$ to be subtracted from the output voltage of the sensor branch. In this way, the common-mode undesired effects introduced by the setup were rejected at the output. Moreover, the gain of the transimpedance amplifier of the reference branch can be adjusted to partially compensate the output measured amplitude, given that the amplitude variations introduced by the GMI sensor used to be small compared to the total voltage swing. Thus, higher voltage variations can be obtained at V_{out} by introducing an extra gain in the final subtractor.

The response of the final decoder system (V_{out}) was initially calibrated under controlled conditions. For that, the 10 mm annealed wire was located at the center of the Helmholtz coils and submitted to *H* field. For comparison, the GMI voltage of the 10 mm annealed wire was similarly characterized under the previous voltage divider (*V*) configuration. The *V* analysis (inset of Fig. 6) shows a displacement of the maxima towards higher magnetic fields, *H* (−378 A/m and 368 A/m) respecting the initial 5 cm in length wire. Besides, a clear diminution in the mean sensitivity of the sensor was produced, concretely almost two orders of magnitude, reducing its value to 6×10^{-5} V/Am^{-1} (or 4.8×10^{-3} V/Oe). These effects can be ascribed to the well-known existence of a critical length in the GMI response. This fact is the result of the increasing role of the closure domains that appear at the ends of the sample after cutting the wire, causing a modification in the magnetic domain structure of the sample [30], [31] and consequently, in its characteristic transverse magnetic permeability. This noticeable decrease represents a trade-off between sensitivity and suitable dimensions for potential applications. In this sense, longer wires exhibit a much larger capacity of detection, however, the shrinkage of components is a required requisite that cannot be disregarded for practical purposes. In any case, further analyses for sensing wire optimization should be addressed in the search for sensitivity improvement i.e. differential sensing configuration [32], non-linear GMI effects, use of GMI phase-based detectors, since they exhibit larger sensitivities when compared to GMI magnitude-based detectors, even at low samples lengths, i.e. 1 cm [33–36], etc. As expected, the previously mentioned displacement in the voltage peaks towards higher *H* was also found for the calibrating curve (see Fig. 6). This curve, in the low field region, displays a continuous increase of V_{out} reching a maximum value around $H \approx 375$ A/m. Under the settled electronics gain parameters, a final mean sensitivity of 3×10^{-3} V/Am^{-1} (or 0.24 V/Oe) for the selected operation point was found in the final decoder system.

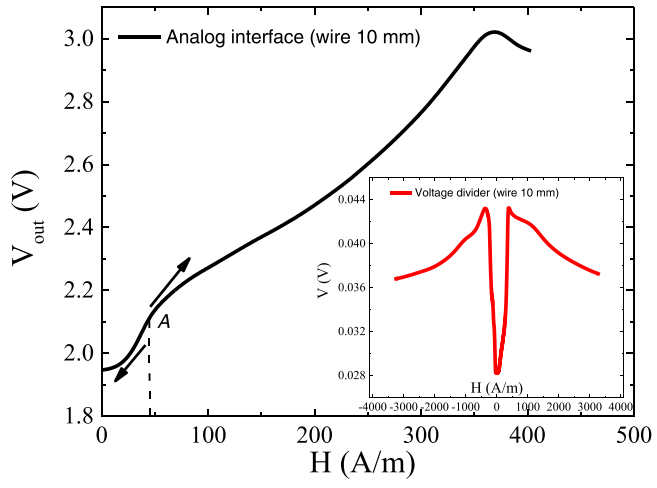

Fig. 6. Electronic sensor interface output signal, V_{out}, versus applied magnetic field, *H* for the 10 mm annealed wire. Inset: Wire response, *V*, versus *H* under voltage divider configuration.

2.5. Scanning of the 3D printed piece: decoding stage

Then, the sensing wire was fixed to a standard glass cover used in microscopy with a square-shaped form, 15 mm side and 0.2 mm thickness. The ensemble was located over the 3D printed piece with the sensor axis along the *x*-direction (see Fig. 3). The scanning was performed along the *y*-direction with a step of 0.5 mm from the initial position at $y = 0mm$ until the final position, $y = 18mm$, beyond the piece upper limit at $y = 16mm$ (see Fig. 3). The movement was transmitted through an adapted commercial 3D printer motor (Artillery Sidewinder x1). A computer using LabView 2014 was employed both for the barcode scanning and the acquisition of the sensor output signal, V_{out}, through a multimeter HP34401A (see Fig. 7). Two different situations were analyzed: i) detection of the MNPs for the as-printed piece and ii) after the application of an external magnetic field, H_{elec}, applied to the whole piece along the *x*- direction. For the initial configuration i), different distances *z* were used. The lowest analyzed distance was $z = 0.3mm$ corresponding to the glass cover thickness plus an extra distance to avoid physical contact. This is the employed distance when no further detail is given. For ii) the magnetic field, $H_{elec} = 0\frac{kA}{m}, 60\frac{kA}{m} and 100\frac{kA}{m}$, was generated by an electromagnet (Applied Magnetics Laboratory, 4H2–45). Notice that this pre-magnetizing field was applied before the scanning measurements.

In order to analyze the possible effect of the direction of the MNPs field on the decoder system, an external and positive magnetic field close to 40 A/m was applied during the scanning stage. From that point (labeled as *A* in Fig. 6), the application of a positive or negative field would produce, respectively an increase or a decrease in V_{out} (see arrows in Fig. 6). Attending to Fig. 1, this magnetic field does not affect the MNPs since much higher fields are required for the change in their magnetization.

3. Results and discussion

First, the capacity of detection of the proposed decoder system

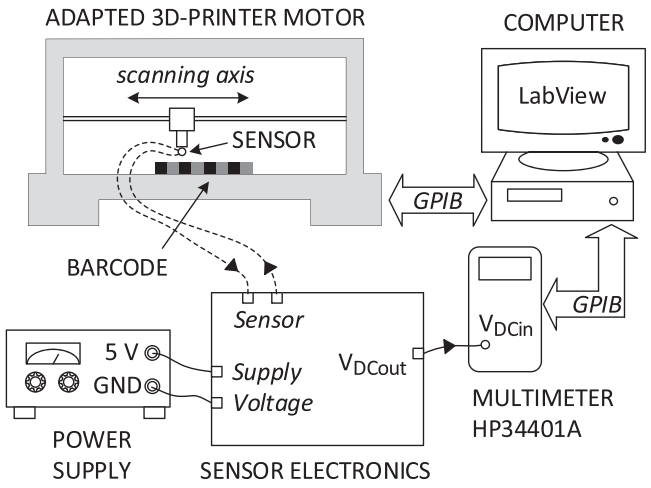

Fig. 7. Scheme of the complete experimental setup.

(sensor nucleus and electronic sensor interface) was checked. In this analysis, the distance z was kept constant at 0.3 mm. This starting configuration represents what hereinafter is called the "initial position", 0°. Moreover, for the sake of clarity, all shown figures incorporate two grey bars at the position of the strips filled with MNPs. can be observed in Fig. 8a, starting from $y \approx 0mm$, a clear increase of V_{out} happened as the sensor approached to the MNPs area, in such a way that, a maximum is obtained in the center of the first MNPs strip (labeled as 1 in Fig. 8a). Then, a gradual decrease in V_{out} resulted until reaching a relative minimum in the region between the magnetic strips ($y \approx 10mm$, center of the polymeric strip). An equivalent behavior was found beyond that position for the second MNPs strip (labeled as 2 in Fig. 8a. It is important to note that V_{out} displays larger values at the center of the empty polymeric strip between magnetic bars, ($y \approx 10mm$, $V_{out} = 2.0987V$) than at the center of the first polymeric strip, ($y \approx 2mm$, $V_{out} = 2.0963V$), and the final measured point, ($y \approx 18mm$, $V_{out} = 2.0947V$, although all related positions are equally separated from the closest magnetic strip. This situation can be interpreted in terms of the capacity of the GMI sensor to sense the magnetic field of the embedded MNPs at a certain distance. While relative voltage differences of $\Delta V = 5.5mV$ and $4mV$ (see Fig. 8a) were respectively found between the two maxima and the minimum at $y \approx 10mm$, higher variations close to 8 mV were observed between those maxima and the adjacent minima situated at $y \approx 2mm$ and at $y \approx 18mm$. Attending to the device sensitivity, these values corresponded to relative variations of the sensed magnetic field of $\Delta H =$ 1.8 A/m, 1.3 A/m and 2.7 respectively, confirming that the sensor experienced a larger magnetic difference when the sensor is only under the "effect" of one magnetic strip.

Then, the sample was rotated 180° (see Fig. 8b). Accordingly, the magnetic field direction and the position of the MNPs strips were altered respecting the initial configuration (see arrows in Fig. 8). Concretely, strip 2 was placed at the position $y =$ 0 mm and initially detected in the scan. As it is shown, two minima in V_{out} were obtained at the center of the MNPs strips ($y \approx 2mm$ and $y \approx 10mm$ respectively), while a relative maximum was found in the region between bars ($y \approx 6mm$). Similarly to the previous case, relative voltage variations of $\Delta V = 6.3mV$ and $4.8mV$ ($\Delta H =$ 2.13 A/m and 1.6 A/m) were found between the minima at and the maximum between magnetic bars voltages values. Moreover, it must be noted the rapid increase in V_{out} ($y \approx 16mm$), linked to the fact that the sensing wire only experienced the effect of one magnetic strip. This fact firstly reveals the feasibility of encoding-decoding information procedure based on 3D printed pieces technology, and secondly, that the prototype is sensitive to the direction of the magnetic field of the particles. Thus, magnetic polarity can also be successfully used to encode information in 3D printed objects. It is important to mention that during the decoding process there is no need of applying an external magnetic field to magnetize the MNPs in the piece, easing the development of a potential final prototype. However, when polarity is analyzed, a biasing field (40 A/m) is required. It is important to note that its intensity was quite low to avoid any change in the magnetization of the MNPs, but enabled the setting of the sensing in an optimal operation point to detect the MNPs field polarity.

One of the main advantages of magnetic codification is the possibility of decoding information without visual contact between code and decoder. So, in many cases, an extra layer of the polymer could be placed on top to completely cover the implemented patterned code. So, in this context, is relevant to determine the range of distances z where the proposed prototype permits the decoding of the information. Fig. 9 shows how the increase of z led to a diminution in the detection capacity, in terms of lower differences between the voltage amplitudes at the maximums and the minimum observed between magnetic strips. In any case, the code can be read until a limit distance of 0.8 mm between the sensor and top surface, revealing the existence of a broad interval where the code is detectable.

Since the employed MNPs are within the limit of superparamagnetic behavior [26] and taking into account the occurrence of particle size dispersion, some nanoparticles could display a certain magnetization at the remanence after being suitably magnetized. To confirm this, the 3D piece was previously submitted to different external magnetic fields, H_{elec}, along the strips axis (positive sense of the x-axis direction, see Fig. 3) to analyze its effect in the detection (see analysis ii) in Section 2.5). The results in Fig. 10 show how the higher the magnetic field applied to the 3D piece, the higher the difference between the two

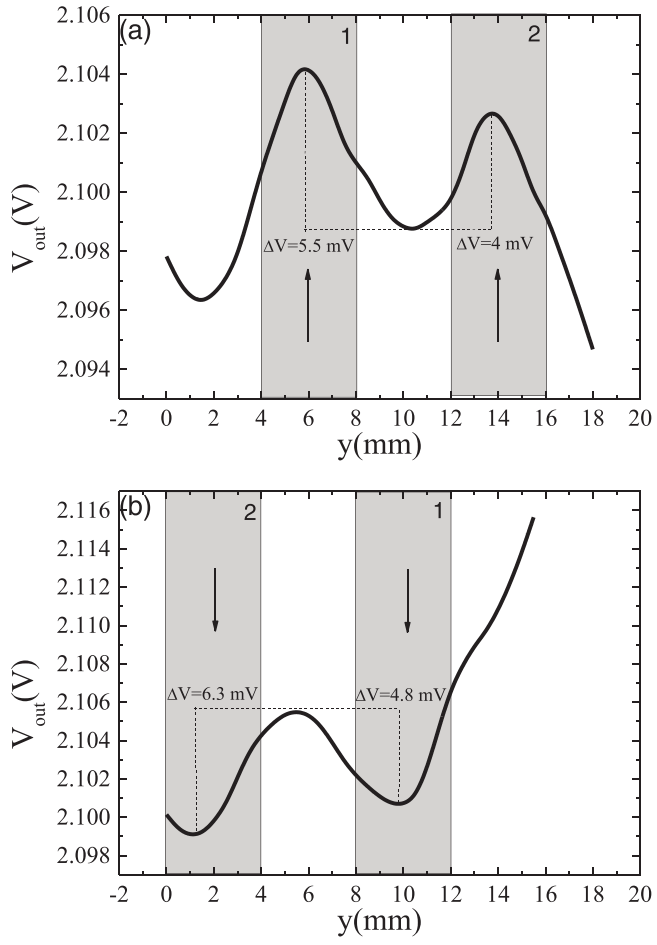

Fig. 8. Variation of the output signal, V_{out}, versus position, y, of the sensor: (a) at the initial position, 0°, and (b) after being rotated 180° the coded strips.

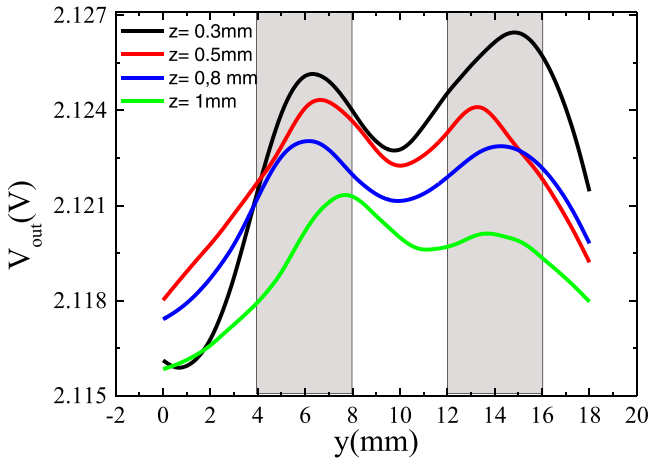

Fig. 9. Variation of the output signal, V_{out}, versus position, y, under different distances z between sensor and piece surface.

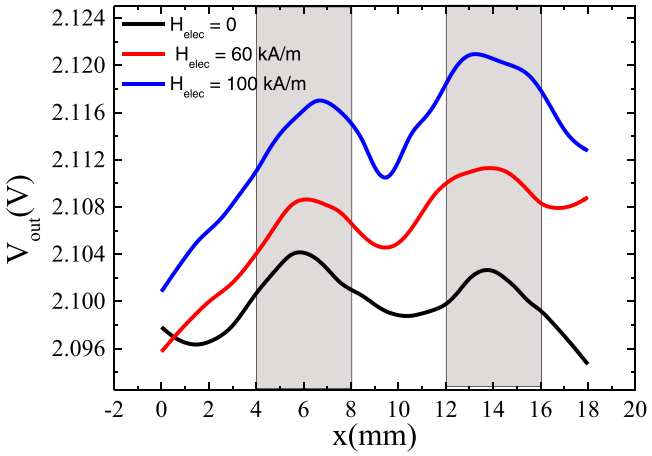

Fig. 10. Variation of the output signal, V_{out}, versus position, y, under different magnetic fields previously applied to the piece.

maximums and the minimum between the magnetic strips. This behavior can be interpreted in terms of the previous magnetization of the MNPs, and the achievement of higher remanent magnetization of the MNPs assembly as H_{elec} was increased. In fact, as the inset of Fig. 1 shows, the increase in the maximum applied magnetic field in the MNPs hysteresis loops, gave rise to an increment of the magnetization at the remanent state. It is important to note that the chosen magnetic fields in these minor hysteresis loops are the same as those applied by the electromagnet. In consequence, a gradually increasing MNPs stray field acted on the sensing wire, enabling an improvement in the decoding process. So, from a practical point of view, a permanent magnet can be incorporated into the proposed potential prototype to improve and ease the decoding process.

The noticed detection improvement in Fig. 10 would confirm the GMI effect as the main origin in the detection of the MNPs through their stray magnetic field. Nevertheless, to discard other contributions in the detected changes of the wire impedance (i.e. changes in the mutual inductance), the evolution of V_{out} was characterized under the simultaneous effect of H (Helmholtz coils) and the embedded MNPs in the 3D piece after being magnetized in the electromagnet at $H_{elec} = 100\frac{kA}{m}$. For that, the sensing wire was aligned over the center of strip 1 (x- direction) and the whole system was placed in the center of the Helmholtz coils. Keeping the wire fixed, two different positions of the 3D piece were analyzed, i.e. the initial (0°) and after its 180° rotation. As is shown in the inset of Fig. 11, an almost symmetrical shift of V_{out}, close to 15 A/m, with respect to the initial calibrating curve (without the effect of the MNPs) was detected. More interesting is the change in the displacement (positive or negative) depending on the orientation of the MNPs orientation respecting the sensor axis. This displacement should be interpreted as an effective magnetic field acting on the sensor, superimposed on the externally applied, H by the Helmholtz coils. The observed dependence of V_{out} on the previous magnetizing field and especially on the *direction* of the magnetic strips joined to the contactless detection procedure, justify that the detection is the result of the effect of the MNPs magnetic stray field on the sensing wire impedance.

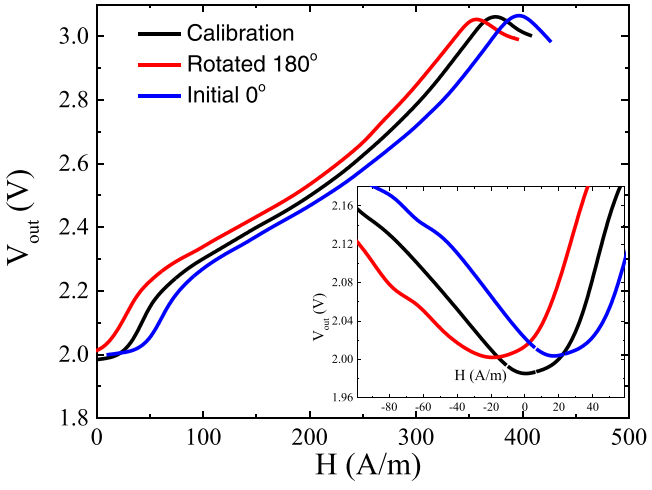

Fig. 11. Evolution of V_{out} versus external magnetic field under the absence of MNPs (calibrating) and the effect of embedded MNPs in strip 1 at initial (0°) and rotated position (180°). Inset. Zoom of the close to $H = 0$ region.

A similar behavior was observed in a previous work [25] where a detection platform for the contactless and reusable detection of magnetic nanoparticles was developed. In this study, the larger size of the employed MNPs (mean diameter of 140 nm) led to a larger MNPs remanence after the application of the magnetizing field, H_{elec} and so, more favorable detection conditions. In this work, the lower mean size of the targeted MNPs proposed a more exigent scenario, that, enabled to test the proposed system under tougher detection conditions. For that reason, it was required an initial treatment of the sensor nucleus to enhance its response at low external magnetic fields, H, as those generated by the MPNs.

Finally, this work intends to demonstrate whether a low-cost and versatile codification-decoding based on the coupling of the 3D printing technique and the GMI effect can be developed. So, from this initial approach, a subsequent optimization process must be tackled to enable the whole device size reduction (magnetic and polymeric strips and sensor). This can be achieved from a double perspective, namely, i) improvement of the magnetic signal of the embedded MNPs by analyzing different compositions, sizes, etc. searching for larger remanences… and ii) enhancement of the GMI sensing element performance where, as previously mentioned, the use of non-linear effects and/or GMI phase-based devices in differential sensing arrangements would permit to gain sensitivity of detection even at the low required sensing element lengths.

4. Conclusions

A magnetic binary encoding system using 3D printing technology is developed. For this purpose, commercial magnetite nanoparticles were embedded in a polymeric matrix of Polylactic Acid (PLA) and Poly-ε-caprolactone (PCL). Then, a printable 3D filament was fabricated and successfully employed for printing a 3D barcoded piece with magnetically encoded information.

A GMI-based prototype decoder has been proposed, based on an amorphous soft magnetic wire of nominal composition $(Co_{0.94}\,Fe_{0.06})_{72.5}\,Si_{12.5}\,B_{15}$. Besides, for the sensor nucleus excitement and signal conditioning, a homemade low-cost electronic was designed. The complete decoding system has demonstrated the capacity of detecting the low presence of the embedded MNPs (5% wt) even without any previous magnetization and in a moderately long range of distances between the sensor and the top piece surface. Additionally, the detection capacity can be improved with a previous magnetization of the encoded piece. Finally, the GMI effect involvement in the decoding process is confirmed.

A low-cost complete magnetic coded-decoded system is proposed, demonstrating the feasibility of the employed coupled techniques for addressing both the manufacturing and decoding stages. This first approximation paves the way for further studies to optimize the 3D manufactured pieces, the GMI sensing wire and homemade electronics performance to tackle the reduction of the elements and the time of detection.

CrediT authorship contribution statement

Juan Jesús Beato López: Conceptualization, Methodology, Measurements, Validation, Formal analysis, Investigation, Data curation, Writing – original draft, Writing – review & editing. **José María Algueta Miguel**: Development of Electronic sensor interface, Writing – review & editing. **Itziar Galarreta Rodriguez:** 3D filament design, fabrication and characterization, Writing – review & editing. **Eneko Garaio:** 3D filament design and characterization, Software. **Alberto López:** 3D filament design and characterization. **Cristina Gómez Polo**: Data curation, Formal analysis, Writing review and editing. **Maite Aresti:** 3D piece printing, Project Administration, Writing – review & editing. **Eneko Soria:** 3D piece printing, Data curation. **Ignacio Pérez de Landazábal:** Conceptualization, Methodology, Validation, Resources, Funding acquisition, Project Administration, Writing – review & editing.

Declaration of Competing Interest

The authors declare that they have no known competing financial interests or personal relationships that could have appeared to influence the work reported in this paper.

Data Availability

No data was used for the research described in the article.

Acknowledgments

This work has been funded by the Gobierno de Navarra - Departamento de Desarrollo Económico within the framework of the Project: “Advanced Manufacturing of Electronics, AMELEC”. It has also been partially funded by the Spanish Government - Ministerio Ciencia-Innovación (PID2019–107258RB-C32 of MCIN/AEI/10.13039/501100011033). Open access funding provided by Universidad Pública de Navarra. The authors also want to acknowledge the Technological Center specialized in mobility and mechatronics of Navarra (NAITEC), for supplying the 3D printed piece and Prof. M. Vázquez (ICMM, Madrid Spain) for kindly supplying the soft magnetic wires.

References

[1] G. Chatzipirpiridis, et al., 3D printing of thermoplastic-bonded soft- and hard-magnetic composites: magnetically tuneable architectures and functional devices, Adv. Intell. Syst. vol. 1 (6) (2019) 1900069, https://doi.org/10.1002/aisy.201900069.
[2] C. Zhang, et al., 3D printing of functional magnetic materials: from design to applications, Adv. Funct. Mater. vol. 31 (34) (2021) 2102777, https://doi.org/10.1002/adfm.202102777.
[3] W. Hu, G.Z. Lum, M. Mastrangeli, M. Sitti, Small-scale soft-bodied robot with multimodal locomotion, Art. no. 7690, Nature vol. 554 (7690) (2018), https://doi.org/10.1038/nature25443.
[4] T. Xu, J. Yu, X. Yan, H. Choi, L. Zhang, Magnetic actuation based motion control for microrobots: an overview, Art. no. 9, Micromachines vol. 6 (9) (2015), https://doi.org/10.3390/mi6091346.
[5] W. Xu, et al., Review of fiber-based three-dimensional printing for applications ranging from nanoscale nanoparticle alignment to macroscale patterning, ACS Appl. Nano Mater. vol. 4 (8) (2021) 7538–7562, https://doi.org/10.1021/acsanm.1c01408.
[6] X. Li, et al., Limpet tooth-inspired painless microneedles fabricated by magnetic field-assisted 3D printing, Adv. Funct. Mater. vol. 31 (5) (2021) 2003725, https://doi.org/10.1002/adfm.202003725.
[7] C. Liu, et al., 3D printing technologies for flexible tactile sensors toward wearable electronics and electronic skin, Polymers vol. 10 (6) (2018), E629, https://doi.org/10.3390/polym10060629.
[8] J.T. Muth, et al., Embedded 3D printing of strain sensors within highly stretchable elastomers, Adv. Mater. vol. 26 (36) (2014) 6307–6312, https://doi.org/10.1002/adma.201400334.
[9] M. Petretta, et al., Multifunctional 3D-printed magnetic polycaprolactone/hydroxyapatite scaffolds for bone tissue engineering, Polymers vol. 13 (21) (2021) 3825, https://doi.org/10.3390/polym13213825.
[10] B.I. Oladapo, S.A. Zahedi, A.O.M. Adeoye, 3D printing of bone scaffolds with hybrid biomaterials, Compos. Part B: Eng. vol. 158 (2019) 428–436, https://doi.org/10.1016/j.compositesb.2018.09.065.
[11] N. Lazarus, S.S. Bedair, G.L. Smith, Creating 3D printed magnetic devices with ferrofluids and liquid metals, Addit. Manuf. vol. 26 (2019) 15–21, https://doi.org/10.1016/j.addma.2018.12.012.
[12] P. Kanitthamniyom, A. Zhou, S. Feng, A. Liu, S. Vasoo, Y. Zhang, A 3D-printed modular magnetic digital microfluidic architecture for on-demand bioanalysis, Art. no. 1, Microsyst. Nanoeng. vol. 6 (1) (2020), https://doi.org/10.1038/s41378-020-0152-4.
[13] A.P. Taylor, C. Vélez Cuervo, D.P. Arnold, L.F. Velásquez-García, Fully 3D-printed, monolithic, mini magnetic actuators for low-cost, compact systems, J. Micro Syst. vol. 28 (3) (2019) 481–493, https://doi.org/10.1109/JMEMS.2019.2910215.
[14] N. Martelli et al., Advantages and disadvantages of 3-dimensional printing in Surg.: A Syst. Rev.,” *Surg.* vol. 159 6 Jun. 2016 1485 1500 doi: 10.1016/j.surg.2015.12.017.
[15] X. Wang, M. Jiang, Z. Zhou, J. Gou, D. Hui, 3D printing of polymer matrix composites: a review and prospective, Compos. Part B: Eng. vol. 110 (2017) 442–458, https://doi.org/10.1016/j.compositesb.2016.11.034.
[16] T.D. Ngo, A. Kashani, G. Imbalzano, K.T.Q. Nguyen, D. Hui, Additive manufacturing (3D printing): a review of materials, methods, applications and challenges, Compos. Part B: Eng. vol. 143 (2018) 172–196, https://doi.org/10.1016/j.compositesb.2018.02.012.
[17] M. Attaran, The rise of 3-D printing: The advantages of additive manufacturing over traditional manufacturing, Bus. Horiz. vol. 60 (5) (2017) 677–688, https://doi.org/10.1016/j.bushor.2017.05.011.
[18] M.-H. Phan, H.-X. Peng, Giant magnetoimpedance materials: fundamentals and applications,”, Art. no. 2, Prog. Mater. Sci. vol. 53 (2) (2008), https://doi.org/10.1016/j.pmatsci.2007.05.003.
[19] K. Mohri, et al., Amorphous wire and CMOS IC-based sensitive micromagnetic sensors utilizing magnetoimpedance (MI) and stress-impedance (SI) effects, Art. no. 5, IEEE Trans. Magn. vol. 38 (5) (2002), https://doi.org/10.1109/TMAG.2002.802438.
[20] G.V. Kurlyandskaya, M.L. Sánchez, B. Hernando, V.M. Prida, P. Gorria, M. Tejedor, Giant-magnetoimpedance-based sensitive element as a model for biosensors, Art. no. 18, Appl. Phys. Lett. vol. 82 (18) (2003), https://doi.org/10.1063/1.1571957.
[21] G.V. Kurlyandskaya, et al., Giant magnetoimpedance biosensor for ferrogel detection: Model system to evaluate properties of natural tissue, Art. no. 19, Appl. Phys. Lett. vol. 106 (19) (2015), https://doi.org/10.1063/1.4921224.
[22] A. Amirabadizadeh, Z. Lotfollahi, A. Zelati, Giant magnetoimpedance effect of Co68.15 Fe4.35 Si12.5 B15 amorphous wire in the presence of magnetite ferrofluid, J. Magn. Magn. Mater. vol. 415 (2016) 102–105, https://doi.org/10.1016/j.jmmm.2015.11.029.
[23] J.J. Beato-López, J.I. Pérez-Landazábal, C. Gómez-Polo, Magnetic nanoparticle detection method employing non-linear magnetoimpedance effects, Art. no. 16, J. Appl. Phys. vol. 121 (16) (2017), https://doi.org/10.1063/1.4981536.
[24] J.J. Beato-López, J.I. Pérez-Landazábal, C. Gómez-Polo, Enhanced magnetic nanoparticle detection sensitivity in non-linear magnetoimpedance-based sensor, Art. no. 21, IEEE Sens. J. vol. 18 (21) (2018), https://doi.org/10.1109/JSEN.2018.2868860.
[25] J.J. Beato-López, J.M. Algueta-Miguel, C. Gómez-Polo, Contactless magnetic nanoparticle detection platform based on non-linear GMI effect, Measurement vol. 180 (2021), 109602, https://doi.org/10.1016/j.measurement.2021.109602.
[26] A.G. Kolhatkar, A.C. Jamison, D. Litvinov, R.C. Willson, T.R. Lee, Tuning the magnetic properties of nanoparticles, Art. no. 8, Int. J. Mol. Sci. vol. 14 (8) (2013), https://doi.org/10.3390/ijms140815977.
[27] E.M. Palmero, et al., Composites based on metallic particles and tuned filling factor for 3D-printing by fused deposition modeling, Compos. Part A: Appl. Sci. Manuf. vol. 124 (2019), 105497, https://doi.org/10.1016/j.compositesa.2019.105497.
[28] P. Sarkar, R.K. Roy, A.K. Panda, A. Mitra, Optimization of process parameters for developing FeCoSiB amorphous microwires through in-rotating-water quenching technique, Appl. Phys. A vol. 111 (2) (2013) 575–580, https://doi.org/10.1007/s00339-012-7260-4.
[29] C. Gómez-Polo, M. Vázquez, M. Knobel, Rotational giant magnetoimpedance in soft magnetic wires: Modelization through Fourier harmonic contribution, Art. no. 2, Appl. Phys. Lett. vol. 78 (2) (2001), https://doi.org/10.1063/1.1336814.
[30] T. Reininger, H. Kronmüller, C. Gomez-Polo, M. Vazquez, Magnetic domain observation in amorphous wires, J. Appl. Phys. vol. 73 (10) (1993) 5357–5359, https://doi.org/10.1063/1.353730.
[31] J.J. Beato-López, I. Royo-Silvestre, C. Gómez-Polo, Micrometric non-contact position magnetoimpedance sensor, J. Magn. Magn. Mater. vol. 465 (2018) 489–494, https://doi.org/10.1016/j.jmmm.2018.05.042.
[32] P.A.D. Riveros, E.C. Silva, S. Pacheco, L.S.B. Cabrera, C.R.H. Barbosa, Design, implementation and experimental characterisation of a high sensitivity GMI gradiometer with an interference compensation system, IET Sci. Meas. Technol. vol. 14 (6) (2020) 688–694, https://doi.org/10.1049/iet-smt.2019.0374.
[33] E.C. Silva, L.A.P. Gusmão, C.R.H. Barbosa, E.C. Monteiro, F.L.A. Machado, High sensitivity giant magnetoimpedance (GMI) magnetic transducer: magnitude versus phase sensing, Art. no. 3, Meas. Sci. Technol. vol. 22 (3) (2011), https://doi.org/10.1088/0957-0233/22/3/035204.
[34] E.C. Silva, L. a P. Gusmão, C.R.H. Barbosa, E.C. Monteiro, Electronic approach for enhancing impedance phase sensitivity of GMI magnetic sensors, Art. no. 6, Electron. Lett. vol. 49 (6) (2013), https://doi.org/10.1049/el.2012.3018.
[35] E.C. Silva, L.A.P. Gusmão, C.R.H. Barbosa, E.C. Monteiro, An enhanced electronic topology aimed at improving the phase sensitivity of GMI sensors, Meas. Sci. Technol. vol. 25 (11) (2014), 115010, https://doi.org/10.1088/0957-0233/25/11/115010.
[36] L.S. Benavides, E.C. Silva, E.C. Monteiro, C.R.H. Barbosa, High sensitivity pressure transducer based on the phase characteristics of GMI magnetic sensors, Art. no. 3,

Meas. Sci. Technol. vol. 29 (3) (2018), https://doi.org/10.1088/1361-6501/aaa27f.

J. J. Beato-López was born in Jerez de la Frontera, Spain. He received an M.Sc. degree from the University of Cádiz, Spain, in 2011. Then in 2018, he received the Ph.D. degree in physics (materials science) from the Public University of Navarre, Pamplona, Spain, where he became a Doctor Assistant Professor. His main research interests are related to the study of magnetic properties in materials and their application to the design of sensors.

José María Algueta Miguel received the Telecommunications Engineering and Ph.D. degrees from the Public University of Navarra, Spain, in 2008 and 2012 respectively. Currently, he is a researcher with the same university. He has been an invited researcher with the University College Dublin (UCD), Dublin, Ireland, in 2011, with the New Mexico State University, Las Cruces (NM), USA, in 2013, and with the INAOE, Puebla, Mexico, in 2015. His main research interests are related to low-power low-voltage analog design, mixed-mode electronic systems and sensor interfaces.

I. Galarreta-Rodriguez was born in Pamplona, Spain. She received an M.Sc. degree from the University of the Basque Country, Spain, in 2016. Then in 2022, he received the Ph.D. degree in Material Science and Technology from the University of the Basque Country, Bilbao, Spain. Her research interest are related to the preparation and study of magnetic nanomaterials and printable magnetic composites.

Alberto López-Ortega was born in Barcelona, Spain. He received the bachelor degree in Chemical Science from the Universitat de Barcelona, Spain, in 2007 and the Ph.D. in Material Science from the Universitat Autònoma de Barcelona, Spain, in 2012. After three postdoctoral contracts (Italy and Spain) he joined the Public University of Navarre in 2020 becoming an associate professor in 2022. His research lines are based on the development of new nanostructured magnetic materials to address current technological requirements, highlighting both the study of the mechanisms that govern their growth process and their fundamental properties.

Eneko Garayo Urabayen was born in Pamplona, Navarre. He completed his degree in Physics at the Public University of Basque Country (UPV/EHU) in 2009. Afterwards, in 2015, he obtained his Ph. D. presenting a doctoral thesis entitled "*Development of experimental techniques for magnetic hyperthermia therapy*". In 2017 he started working as Doctor Assistant Professor at the Public University on Navarre (UPNA). His main research interests are related to the study of magnetic properties in nanoparticles and their applications.

Cristina Gómez-Polo was born in Madrid, Spain. She received the M.Sc. and the Ph.D. degrees in Physics (Material Science) from the Complutense University, Madrid, Spain, in 1988 and 1992, respectively. In 1995 she joined the Public University of Navarre as a lecturer and become full professor in 2011. Her research activity is mainly focused on the magnetic properties and applications of nanostructured magnetic materials and includes the study of amorphous, nanocrystalline and nanoparticle systems.

Maite Aresti was born in Santurce, Spain. She received the M.Sc. degree in Chemistry from the University of the Basque Country, San Sebastian. In 2017, she received the Ph.D. degree in Materials Science from the Public University of Navarra, Pamplona. She currently works at NAITEC (Technological Center of Automotive and Mechatronics) as a project manager. Her research activity is focused on the development of new materials for 2D and 3D printed electronics.

Eneko Soria-Picón. Graduated in mechanical engineering at UPNA University in 2018. Currently projects and services technician at the NAITEC technology centre in the area of additive manufacturing since 2020.

Pérez-Landazábal: was born in Vitoria-Gasteiz, Spain and received the Ph.D. degree in solid-state physics from the Basque Country University in 1995. He is full Professor in the Science Department of the Public University of Navarra, Pamplona, Spain and researcher of the Institute for Advanced Materials and Mathematics (InaMat^2). His research interests include ferromagnetic shape memory alloys, magnetic sensors and actuators and magnetic nanoparticles for medical applications. Nowadays, his activity is mainly focused on microstructural and magnetic characterization, phase transformations and defects in solids.